Design and Minimization of Mutual Coupling Steered Array Lens Antenna for 5G Communication

ROOPASHREE D.[1], SHRUTHI. K. N.[1], R. BHAGYALAKSHMI[1], CHAITHRA K. N.[2]
[1]Department of Electronics and Communication, Government Engineering College, Hassan, INDIA
[2]Department of Electronics and Communication, NITTE Institute of Technology, Bangalore INDIA

*Abstract***:** Examining and evaluating the improved microstrip patch antenna to enhance the performance by the initial objectives are the main contribution of this paper. To achieve multiband operation, the patch's shape is first adjusted later microstrip patch with the slot presented. With the help of the Ansoft HFSS antenna simulator, functional analysis has been shown to examine the impact on antenna resonant frequency. A probe-driven microstrip patch antenna imprinted on FR4 epoxy substrate with 1.6mm thickness and a dielectric constant of 4.4 is developed in this work via the HFSS tool for wireless applications operating between 2 to 5GHz. To achieve multiband operation, the structure of the patch is varied. The impacts on antenna resonant frequency are examined through numerical simulations. The length, as well as the width of a traditional patch antenna, is initially computed, and further, an appropriate patch dimension of 28.3mm x 36.9mm has been determined. For multiband operation over the frequency ranging between 2 and 5GHz wireless applications, a probe-driven microstrip patch antenna imprinted on FR4 epoxy substrate with 1.6mm thickness and a dielectric constant of 4.4 is built via the HFSS tool. The proposed architecture of a traditional microstrip patch antenna is imprinted on an FR4 epoxy substrate with a 1.6mm thickness and a 4.4 dielectric constant. The proposed antenna design is illustrated for the 3D structure of the Mutual Coupling Steered Array-Lens Antenna System (MPA) with an improved patch. To achieve multiband operation, two slots are inserted on the edges of the patch, and both the slots are 2mm wide, as well as the depth of the slots is modified to see how it corresponds to the resonant frequency. This work is mainly concentrated on (i) Examining as well as evaluating the improved microstrip patch antenna to enhance its performance, (ii) Examining, evaluating, as well as assessing the performance of an improved split ring resonator metamaterial, and (iii) Exploring, analyzing, as well as evaluating the performance of dielectric lens base patch array antennas and (iv) Developing as well as analyzing the transmission line phase shifter. The groundwork for developing this work is being carried out, and a comparative study is made on (i) techniques for improving the antenna's performance through the application of a modified patch antenna, a Modified split ring resonator, a Dielectric lens structure, and Transmission line phase shifter.

Keywords: MPA, Line phase shifter, 5G, Modified patch Antenna, and Microstrip antenna.

Received: October 19, 2021. Revised: October 22, 2022. Accepted: November 24, 2022. Published: December 31, 2022.

1 Introduction

In superior execution airplanes, space apparatus, satellites, rocket applications, portable radio, and remote interchanges where size, weight, cost, execution, simplicity of establishment, and streamlined profile are limitations, low-profile receiving wires might be required. To meet these necessities, Microstrip receiving wires can be utilized. Radiation execution can be improved by using appropriate plan structures. The utilization of high permittivity substrates can scale down Microstrip receiving wire size. Thick substrates with a lower scope of dielectric offer improved proficiency and vast transmission capacity; however, it requires a bigger component size. Microstrip radio wire with a superconducting patch on a uniaxial substrate gives high radiation productivity and gain in millimeter frequencies. The width discontinuities in a Microstrip fix lessen the length of reverberating Microstrip receiving wire Permittivity, Metamaterial, permeability, return loss, MPA, and Mutual coupling steered array and radiation effectiveness also. The appropriate impedance matching throughout the corporate and series taking care of cluster design gives high productivity Microstrip receiving wire.

An Antenna array cluster is a bunch of N spatially isolated antenna wires utilized to coordinate emanated power towards an ideal rakish area. When an exhibit has been intended to concentrate on a specific heading, it turns into a straightforward make-a-difference to guide it toward another course by changing the general periods of the cluster components, which is known as directing or checking. Close to focal points are fundamentally used to collimate episode different energy to keep it from spreading in undesired headings. By appropriately molding the mathematical setup and picking the suitable material for the focal points, they can change different types of disparate energy into plane waves. Exploratory approval of such focal points and extensive finishes by involving horn antenna wires or coaxial-to-waveguide changes as an essential source to enlighten the focal point. Such feed techniques cause an expansion in the profile of the Luneburg focal point by the voluminous size of the taking care design, making in-board reconciliation of such gadgets extremely challenging.
Additionally, the round locus of central marks of such focal points needs to be corrected for beneficiary exhibits, which are, by and large planar. Henceforth represent-day correspondence world examination of the radiation example of the focal points. They use a reasonable methodology and describe the essential radiators that are substantial anywhere in complex, challenging, and fundamental angles. To avoid grating lobes, the gap between elements in steering antennas should be within 0.6. Because the atoms are closer and interact more strongly in this circumstance, the mutual coupling suffers. Many wireless antenna applications demand antennas to have a compact form factor while still having a high gain, substantially higher than an array of the same size. Mutual coupling between antenna array elements is crucial if the element spacing is narrow. It must be quickly considered in the design process, as it can result in substantial degradation in an antenna's overall performance. Many strategies for reducing mutual coupling, such as antenna arrays, have been presented in the literature. To construct a small beamforming lens-fed antenna array at 24 GHz, In [10], the authors proposed a two-layer Rotman lens-fed Microstrip antenna array. In the era of SiP, a multilayer implementation of the lens-fed antenna array would be advantageous, as it is a simple technique to create a beamforming module, [11]. Low profile substrate integrated planar HMFE lens antenna using metamaterial for wideband operation was presented in [12]. For compactness, the authors suggested in [4] combining a typical conical horn antenna with a dielectric flat transmit-array perforated lens.
The focal points give collimation and wide-end guiding and go about as rough. Radom gives successful insurance to the cluster, which is the most appropriate to a sea climate with high directivity. The collimation property of dielectric focal points over a multi-band set of little-size fixed radio wires was discussed. They have likewise planned a Microstrip cluster radio wire with its printed feed network on a solid substrate for the upgrade with a dielectric focal point and acquired further increase, [13] which means a compelling bigger radio wire. Actual conservativeness could now be accomplished by diminishing the number of components in consonance with the collimation given by the focal point, [8], [9]. From that point forward, Metamaterial protection was utilized to alleviate the ascent in standard coupling brought about by the decrease in component distance. Metamaterials are originally arranged composite materials with extraordinary highlights not found in nature. They fostered a basic methodology for diminishing standard coupling between two MTM-roused electrically small receiving wires that are firmly dispersed, [7] rely upon self-scratch-off of the instigated shared ground, are close to handling flows, and require no additional development, [5]. For microwave and optical applications, metamaterials are garnering increasing study interest. Metamaterials are materials that can display electromagnetic properties that are not typically found in naturally existing materials, [1]. Split ring resonators (SSR) are one of many types used in Metamaterial design because they have negative permittivity and permeability around their resonant frequencies. In [2], [3], [4], [5], [6], [7], [8] a range of SRR structures – square, circular, triangular, and elliptical – have been proposed and researched, To produce multi-resonant behavior, single, double, and triple-ring hexagonal and circular-shaped SRRs are built and simulated using MATLAB 2017 and HFSS simulators. Negative permittivity and permeability bandwidths are demonstrated using electromagnetic characteristics, [10].
Based on a detailed literature survey on mutual coupling steered array lenses for different applications, it is concluded that there are many gaps

in the minimization of mutual coupling, mainly in 5G communications, [17]. Mutual coupling plays a significant role in current communication technologies; therefore, this work is majorly concentrated on the design of two rings hexagonal split ring resonator, which is used to design the MPA antenna. One of the ways to minimize mutual coupling is by considering a linear phase shifter, dielectric lens structure, and split ring resonator, [14], [15].

This paper presents a brand-new compact, low-cost patch array antenna with beam steering functionality and mutual coupling reduction between the patches. Beam steering and reduced mutual coupling are made possible by adding a modified hexagonal split ring resonator metamaterial structure in one of the 1 X 2 patch arrays. An antenna array can achieve a mutual coupling reduction of about 4 dB at the operational frequency with patches spaced 0.25 o apart. The left and right produce a beam scanning of -200 to +200 changed patches, respectively. The simulation findings utilizing experimental measurements are used to validate the outcomes of the manufactured prototype antenna. This proposed method for constructing beam steering arrays also lessens the mutual coupling impact between microstrip patch array antennae. It is efficient to perform MPA by altering one of the patches. By changing the left and suitable patches in a 1x2 patch array-based antenna, a +200 and -200 beam tilt can be obtained, with mutual coupling reduced by about 4.5 dB. The proposed antenna is made of inexpensive FR4 epoxy and is suitable for 2.5GHz communication systems, [16].

2 Design of Proposed Two Rings Hexagonal Split Ring Resonator

The main aim of this work is to analyze the metamaterial structure and examine its electrical characteristics. The first objective is to split ring resonator metamaterial with a hexagonal shape, discussed through simulation graphs via the HFSS simulator to verify the electrical factors such as permeability and permittivity. The objective of this work is to design the following.

- To design a metamaterial structure computationally and examine its electrical characteristics.
- Examining the antenna system of the lens.
- Determining the electrical characteristics like permeability, refractive index, and permittivity from a metamaterial framework.
- Design of the lens antenna system.

Table.1. Optimized Results Parameters of two-ring HSRR

Sl. No.	Design parameters	Value Range
1	Height of dielectric substrate	1mm
2	The gap between split rings	0.08mm
3	Width of the strip	0.866mm
4	The radius of the outer polygon	4.75mm

With the help of simulation tools such as Ansoft HFSS, a hexagonal split ring resonator comprising two rings was developed with an operating frequency of 2.6 GHz. Fig.1 represents the schematic geometry, and the fabrication of two HSRR rings with six segments, which are illustrated in Fig. 2. A metal ring produced on a dielectric substrate (FR4) with 4.4 relative permittivity constitutes a structure.

Return Loss Analysis: To compute the HSRR return loss value for two rings, a magnetic field is excited perpendicular to the split ring, and an electric field is closely parallel to the split ring architecture via two-wave ports. A return loss value of -20.8829 dB is obtained when it is done. To achieve an appropriate Return Loss Value, a frequency ranging between 1 and 5 GHz and 401 frequency samples were chosen over this frequency range. Fig.3 illustrates that at 2.6 GHz, a Return Loss of -20.8829 dB is accomplished. The return loss is reduced at the central frequency.

Analysis of Negative permittivity and permeability plot for Two Rings HSRR: Fig.4 illustrates the genuine parts, and Fig.5 illustrates the imaginary parts of permittivity and permeability for a two-ring HSRR. These exhibit a hexagonal-shaped SRR, including a single ring with non-positive absolute effective permittivity and permeability at a frequency of 2.6 GHz. The permittivity and permeability were determined to be -20.8829 and -0.4911, respectively, at this resonant frequency, indicating that the intended structure functions as a left-hand metamaterial. Using the Ansoft HFSS antenna simulator, an NZIM (near zero-index

metamaterial) lens is developed and combined with a standard patch antenna to maximize the gain of an antenna following the first two objectives to analyze as well as implement the lens antenna systems. The broadside efficiency of a Microstrip Patch Antenna for WLAN applications is increased in this work by employing a superstrate structure that is made up of an array of 7X7 metamaterial unit cells. A metal strip is inserted into the typical mirrored S-like shape to produce the suggested metamaterial unit cell. The unit cell examination and parameter extraction via periodic boundary constraints are employed to verify the behavior of the near-zero index. It also demonstrates the substantial decrease in the size of individual cells. Simulation findings show that the gain was increased by 1.56 dB over a typical patch antenna when employing the NZIM (Near Zero Index Metamaterial) lens. The broadside gain of the Microstrip Patch Antenna is increased by utilizing HFSS and a superstar. In the same way, the half-power beam width is reduced by 200 in both E-plane and the H-plane. The following sections examine as well as analyze the results in detail.

Calculating f_0 for SRR in HFSS tool: The resonant frequency of HSRR is approximated using a statistical model. The framework also estimates how the resonance frequency will vary as the angle of rotation between the inner and outer polygons ranges. It has been analytically verified that the resonance frequency of 2.5GHz can be attained.

Empirical Formulae: With the help of the below equation, the Resonant Frequency (f_0) of the HSSRR can be calculated

$$\text{fo} = \frac{1}{(2\pi\sqrt{(2a_{eq}.L_{Net}.C_{Net})})} \quad \ldots (1)$$

Here, the effective radius of HSSRR is represented by a_{eq} and its expression is as follows:

$$a_{eq} = 2a\sin\left\{\frac{\pi}{N}\right\} - \frac{g}{N} \ldots\ldots\ldots\ldots (2)$$

Here N=6, Equivalent inductance is represented by $L_{Net,}$ and its expression is represented as follows:

$$L_{Net} = 0.00508 * \left(2.303\log_{10}\frac{4l}{C} - 2.636\right). (3)$$

Here, the strip width and perimeter are represented by c and respectively, and the expression is illustrated as indicated in the below equation.

$$l = 2.a.N.\sin\frac{\pi}{N} \ldots\ldots\ldots\ldots (4)$$

The equivalent capacitance of the structure is indicated by $C_{Net,}$ and the expression is given as follows:

$$C_{Net} = \left\{\frac{\left(N.\sin\left\{\frac{\pi}{N}\right\}+\beta\right)^2 - \left(\frac{\Delta}{a}\right)^2}{2\left(N.\sin\left\{\frac{\pi}{N}\right\}+\beta\right)}\right\} \ldots\ldots\ldots\ldots (5)$$

Where $\beta = \frac{c_g}{a.c_{pul}}$ and c_{pul} is the capacitance per unit length of the hexagonal SRR

$$\Delta = \alpha\sin\frac{\pi}{N}.(2m+1) - \alpha\cos\left\{\frac{\pi}{N}\right\}.\tan\left\{\frac{\pi}{N} - \varphi\right\} \quad \ldots. (6)$$

Now the upper half-ring (C_u), as well as the lower half-ring (C_l) capacitance, can be simply calculated from Δ as well as C_{Pul} as follows:

$$C_u = \left[N.a.\sin\left\{\frac{\pi}{N}\right\} - \Delta\right].C_{Pul} \ldots\ldots\ldots\ldots (7)$$

And

$$C_l = \left[N.\alpha.\sin\left\{\frac{\pi}{N}\right\} + \Delta\right].C_{pul} \ldots\ldots\ldots\ldots\ldots (8)$$

the capacitance because of split gaps in the rings is indicated by C_g and can be approximated using the equation

$$C_g = \frac{\varepsilon_0.\varepsilon_r.c.h}{g}$$

Here the permittivity of free space $\left(\varepsilon_0 = 8.854 \times 10^{-12}\frac{F}{mt}\right)$ is indicated by ε_0 as well as the relative permittivity is indicated by ε_r and is different for different materials.

Calculating the resonant frequency of HSRR: The necessary dimensions of HSSR can be acquired by specifying the HSRR dimensions or an input parameter employing a MATLAB code; correspondingly, the mat lab code can also be used to determine the HSRR for a specific operating frequency. Initially, the SRR is designed as a single-ring hexagonal-shaped SRR with various side lengths. As illustrated in Fig.1, the side lengths selected for the SRR-1 are 3mm, SRR-2 is 2mm, and SRR-3 is 1mm. A metal ring produced on a dielectric substrate RO4003 with 3.55 relative permittivity constitutes the structure. 8mm x 8mm x 0.81mm is the dimension of the substrate. The metal rings possess a width (w) and gap width (w) of 0.33mm. During SRR modeling, the return loss is considered one of the most significant parameters. Fig. 2 shows the amplitude in dB of the S21 factor for single-ring unit cells such as SRR-1, SRR-2, and SRR-3. The resonance frequency for SRR-1 is 5.1GHz with a length of 1mm; for SRR-2, the resonance frequency is 7.3 GHz with a 2mm length; and for SRR-3 with a side length of 3mm, the resonance frequency was found to be 12.3GHz which is illustrated in Fig.3.

The resonant frequency switches from lower to a higher frequency, i.e., 5Hz to 10GHz whenever the capacitance is reduced. The side length decreases from 3mm to 1mm. As a result, by varying the side length of SRR, one can achieve the necessary shift in frequency. Figure 3 depicts an essential building component of the NZIM superstrate, the metamaterial unit cell, used to enhance MPA gain. These unit cells are printed on a single side of a 0.8mm thick FR4 substrate. Ax = Ay = 4.5 mm, L1=4.2 mm, L2=1.725 mm, L3=1.2 mm, W1=4.3 mm, W2=3.5 mm, W=0.25 mm are the design parameters of the NZIM unit cell with the best possible values for near-zero refractive index performance at 5GHz frequency band. By varying the performance parameters of the NZIM unit cell, the frequency band associated with a near-zero refractive index can also be varied. The unit cell is again simulated using ANSYS HFSS with PEC and PMC boundary constraints. The scattering parameters are used to determine the effective medium properties, such as permittivity, refractive index, and permeability, as illustrated in Fig.6, Fig.7, Fig.8, and Fig.9, respectively. As shown in Figure 5, applying the NZIM unit cell results in a substantial decrease in the unit cell size. The overall antenna system's efficiency has been examined. The gap between the primary patch antenna and the lens has been tuned to minimize the coupling between the patch antenna and the lens. The lens structure is positioned at h = 40 mm above the patch to achieve this. This height is typically $\lambda o/2$, wherein the MPA's operating wavelength is represented by λo. The lens width and length are set to match the patch's broadside radiation for adequate coverage. Figure 6 shows the gain of a Microstrip patch antenna along with an NZIM lens. 4.28 percent and 5.46 dB are the impedance bandwidth and gain of a Microstrip patch antenna that is achieved. The linear plot of the radiation pattern in the E plane and the H plane demonstrates the convergence of the radiated beam, which is illustrated in Fig.10 and Fig.11. HPBW in the H-plane (H) has been reduced from 720 to 510. In contrast, HPBW in the E-plane (E) decreased from 900 to 580. As a result, the idea of gain enhancement by beam convergence is proven.

This work provides a hexagonal-shaped Split Ring Resonator built on Rogers' substrate. Various magnetic resonances specified by different concentric rings in the unit cell induce multi-resonant phenomena in the microwave regime. To analyze and plot the S-parameter of a hexagonal-shaped split ring resonator over a frequency range, the ANSYS HFSS tool is often employed. The required frequency can be achieved by varying the side length of SRR, which is demonstrated through simulation by employing HFSS. The occurrence of non-positive permeability bandwidths is verified using electromagnetic characteristics. The developed HSSRR is considered one of the promising platforms for applying metamaterial in many parts of the electromagnetic spectrum, particularly in device miniaturization. Fig.12 and Fig.13 illustrate the results obtained by integrating SRR-1 and SRR-2 in a hexagonal-shaped SRR with two resonant frequencies. Likewise, a three-ring hexagonal-shaped SRR is built by combining SRR-1, SRR-2, and SRR-3 to obtain a three-resonant frequency. Fig. 14 represents the magnitude spectra of the S21 parameter for two rings, and Fig. 15 illustrates the magnitude spectra of the S21 parameter for three rounds of HSSRR. SRR with two rings resonates at 5.1 GHz and 7.4 GHz frequencies. However, SRR with three rings resonates at 5.1 GHz, 7.5 GHz, and 12.3 GHz frequencies. As a result, multi-band operation is possible. Table. One depicts the resonance frequencies of all hexagonal-shaped structures.

3 Results and Discussions

The dip in Fig. 2 is achieved at 2.4GHz and corresponds to the resonant frequency of the traditional patch antenna. At this frequency, the return loss is -19dB. The antenna absorbs the maximum input energy whenever the return loss is minimal, i.e., minimum reflection. The gain for MPA, simulated via HFSS, is found to be 3.0dB and is illustrated in Fig. 3. This complies with the Microstrip Patch antenna industry benchmark. Two bands of resonant frequencies are produced at 2.45GHz with -15dB return loss, as well as another frequency band at 4.6GHz with -18dB return loss, which is illustrated in Fig. 5. A resonant band is defined as a frequency band possessing a return loss of less than -10dB. The optimized MPA has a gain of 4.6dB, shown in Fig. 6, and when compared to a

traditional patch antenna, the growth is improved by 1 dB.

Furthermore, the slot's length immediately prior to the patch was modified to see how it varies with frequency. Table 1 shows the results, whereas Fig. 7 shows the graph that corresponds to them. The resonant frequency at 4GHz advances towards 5GHz as the length Lx1 is increased from 1mm to 6mm, as shown in Fig. 4. Antenna developers employ this technology to design antennas varying between 2 to 5GHz applications. Furthermore, a slotted single probe feed microstrip patch antenna is presented. The patch consists of a rectangular slot that enables dual-band operation. At a frequency of 2.4 GHz, the primary antenna is being devised with a Wi-Fi system. The antenna developed using HFSS software exhibits excellent characteristics for applications such as wireless communication and S-band ranging from 2 to 5GHz.

Design of a Typical Microstrip Patch Antenna: The traditional patch antenna's length, as well as width, can be estimated. Fig.1 illustrates the configuration of a conventional microstrip patch antenna imprinted on FR4 epoxy substrate with 1.6mm thickness and 4.4. dielectric constant. The dimensions of a patch and substrate are 28.3mm x 36.9mm and 86mm x 96mm, respectively.

Suggested Microstrip Patch Antenna with Slot*:* Fig.2 illustrates a 3-dimensional structure of the suggested MPA that includes a slot. A rectangular space is inserted into the patch to achieve the optimum dual-band operation. The antenna's length and width have been reduced to 4mm x 15mm. The resonant frequency of the typical patch antenna is 2.4GHz, achieved by dip, and is depicted in Fig. 1. At this 2.4GHz frequency, the return loss obtained is -19dB. The antenna receives the maximum input energy whenever the return loss is minimal, i.e., minimum reflection. By employing HFSS, the gain for MPA simulated was found to be 3.0dB, shown in Fig.1. This complies with the Microstrip Patch antenna industry norm. Dual-band operation is described in Fig. 3. The 2.2 GHz is the initial frequency similar to the standard MPA**,** and 4.55 GHz is the subsequent frequency. The return loss observed in these two bands is much lower than the required, i.e., not more than -10dB. Figure 4 shows that the gain attained for the 2.4 GHz band is 3.1dB, which can be acceptable, and a 0.1dB increase in revenue exists.

Parametric Analysis of Microstrip Patch Antenna with Slot*:* After that, to examine the impact on the resonant frequency, the slot length was varied with the specified 2mm slot width. Table 1 illustrates the outcome, whereas Fig. 5 shows the graph that corresponds to that result. Fig.5 demonstrates that whenever the rectangular slot length is modified, there is no variation in the first, i.e., 2.4GHz band, while the resonant frequency surpasses 5GHz in the subsequent band. This information helps antenna engineers identify the suitable frequency band for their applications.

Initially, we demonstrate the application of a modified split ring resonator metamaterial structure to minimize mutual coupling in a Microstrip patch antenna array. The suggested MSRR unit cell comprises two nested rings with two symmetrical splits. At a frequency of 2.4 GHz, the primary microstrip patch antenna is operated, and the distance between the edges of the primary antenna element is 31.5mm and approximately 0.25 λ0. The antenna array isolation is considerably improved by introducing the MSRR Metamaterial structure on the radiating patch of the antenna array placed on the right side. The results obtained from the simulation illustrate that the isolation is minimized by not less than 12 dB and by not affecting the frequency of operation or radiation patterns. Fig.15 outlines the conceptual Microstrip antenna array with MSRR metamaterial structures. The variety of an antenna is constructed on an FR4 with ε_r 4.4, δ=0.02, h = 1.57 mm relative permittivity, loss tangent, and thickness, respectively. Two similar rectangle patch antennas featuring coaxial feeding constitute an antenna array. The antenna array possesses a ground plane at the end. The arrays of antennas are designed to operate at 2.4 GHz and keep 31.5 mm edge-to-edge spacing. As seen in Fig. 15, the MSRR unit cell is made up of two nested rings, and each of these rings consists of two symmetrical splits. The unit cells of MSRR are inserted between the two antennas on the left side with 1 mm spacing between them. L_{gnd} = 70 mm, L = 28.3 mm, W_{gnd} = 130 mm, W = 36.5 mm, r_1 = 2.5 mm, r2 = 2 mm, d = 31.5 mm, d_1 = 0.25 mm, d_2 = 0.25 mm, k = 0.08 mm are the best possible antenna array dimensions to obtain maximum isolation. A simulation model in ANSYS HFSS was used to analyze the efficiency of the suggested MSRR-loaded antenna array.

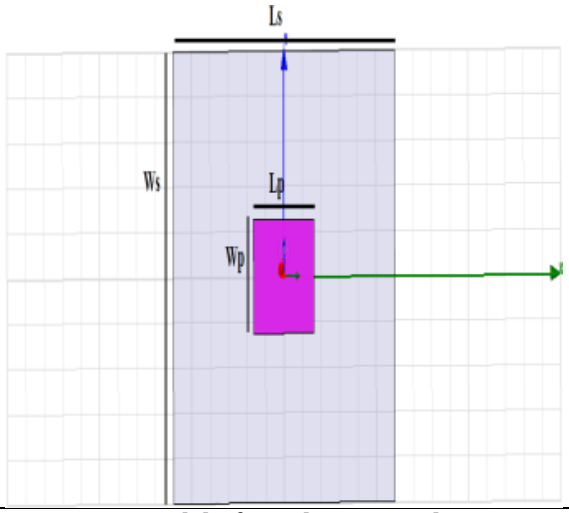

Fig. 1: 3D Model of Single rectangular Microstrip patch Antenna

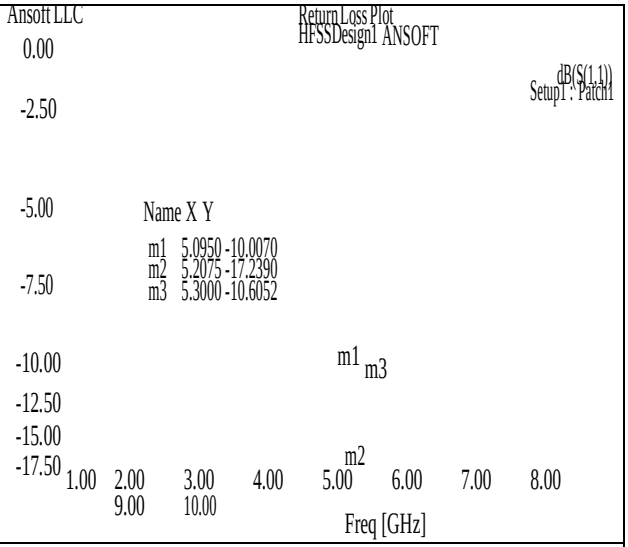

Fig. 2: The plot of the Return loss of Basic patch antenna without NZIM lens

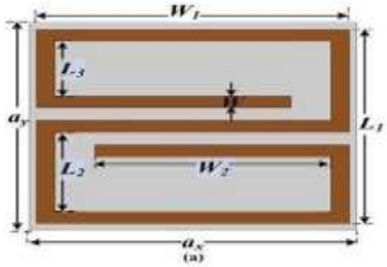

Fig.3: The schematic diagram of the NZIM unit cell

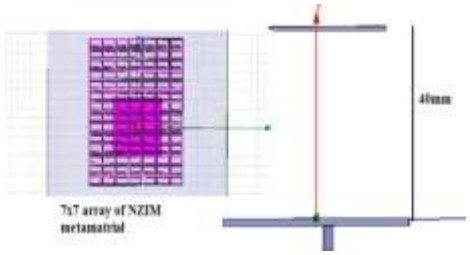

Fig. 4: The schematic diagram of the proposed antenna with NZIM lens: (a) Top view (b) Side view

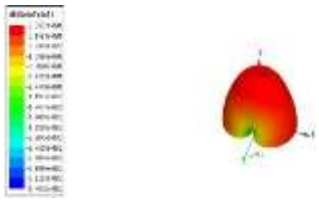

Fig. 5: 3D polar plot of gain of Basic patch antenna without NZIM lens

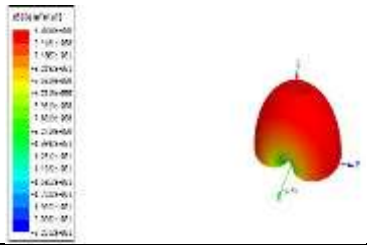

Fig. 6: 3D polar plot of gain of Basic patch antenna with NZIM lens

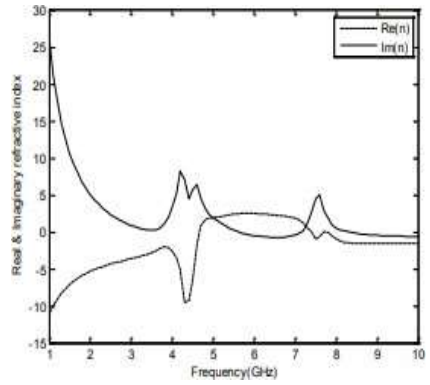

Fig. 7: Extracted Real and Imaginary Part of Refractive Index for the Proposed NZIM Unit Cell

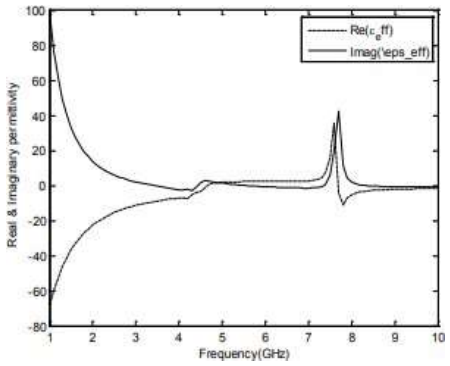

Fig. 8: Extracted Real and Imaginary Part of Permittivity for the Proposed NZIM Unit Cell

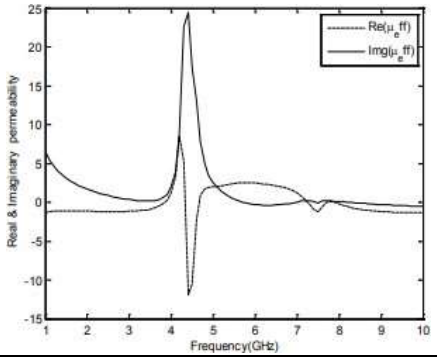

Fig. 9: Extracted Real and Imaginary Part of Permeability for the Proposed Nzim Unit Cell

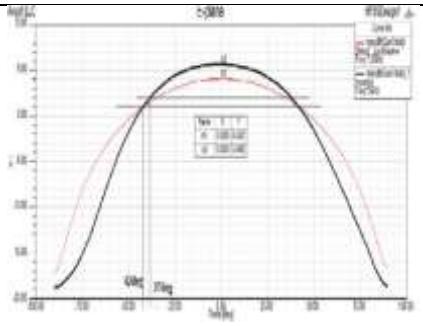

Fig. 10: Simulated Radiation Pattern of Basic Patch Antenna Loaded with Single Layer- E-Plane

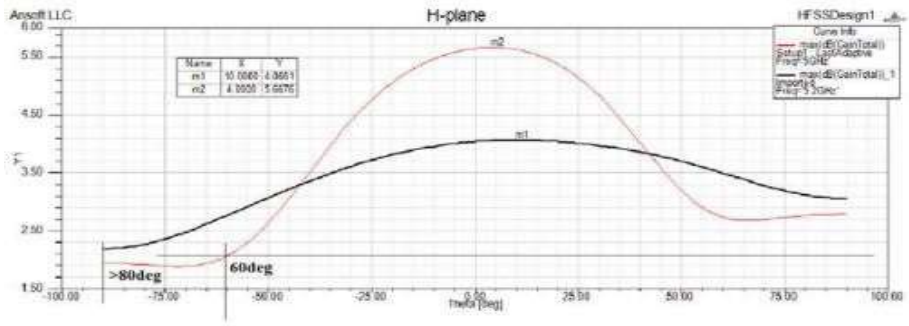

Fig. 11: Simulated Radiation Pattern of Basic Patch Antenna Loaded with Single Layer- H-Plane

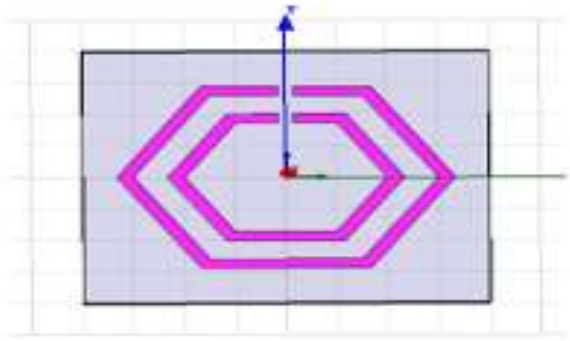

Fig.12. Hexagonal SRR with two concentric rings simulated using HFSS

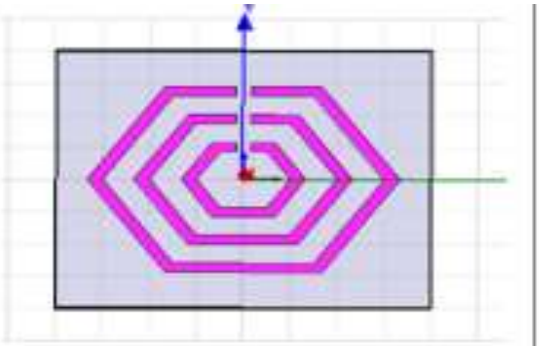

Fig.13. Hexagonal SRR with three concentric rings simulated using HFSS

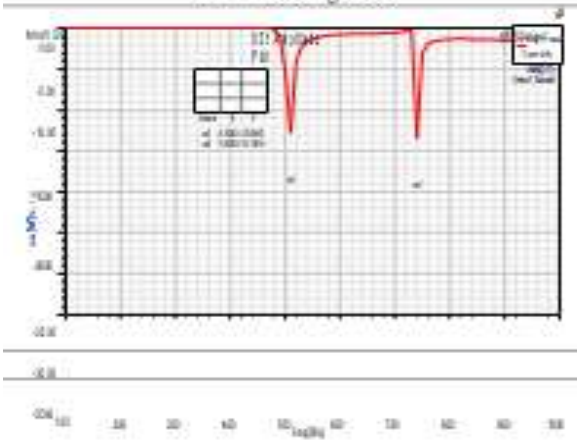

Fig.14. The magnitude of S_{21} for SRR with two rings

Table. 1 Summary of Simulation Results	
Structure	Resonant Frequency in GHz
SRR-1	5.1
SRR-2	7.3
SRR-3	12.3
Two rings	5.1 & 7.4
Three rings	5.1, 7.5, 12.3

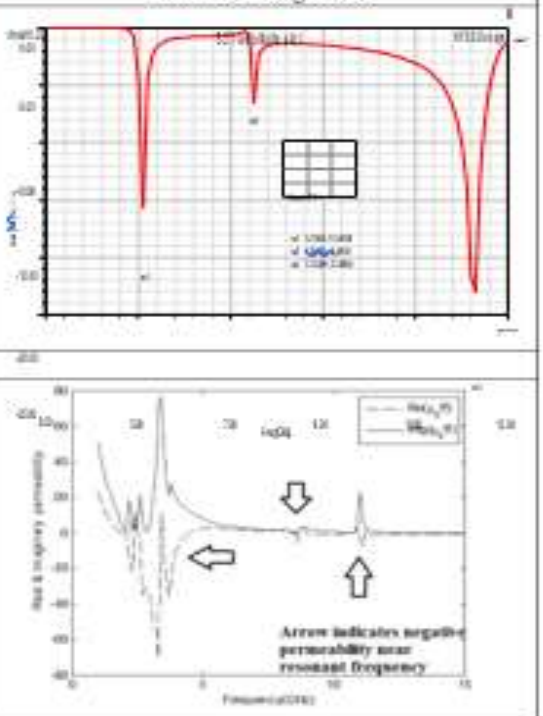

Fig.15 The magnitude of S_{21} for SRR with three rings

To assess the effectiveness of the planned patch-modified antenna array using an MPA structure slot, numerical simulation in ANSYS HFSS is employed. Agilent Technologies' PNA Network Analyzer is used to measure the antennas (E8363C, 10MHz-40GHz). Fig. 3 depicts the experimental configuration for measuring operating frequency. In Fig. 3, the isolation S12 and return loss S11 plots of a patch array antenna without patch modification are shown in simulation and measurement. Similarly, Fig.3 shows the simulated and measured isolation S12 and return loss S11 plot of a left patch adjusted. Once the MSRR structure is positioned on the left side of an antenna array, the current present on the right antenna element is low. A large amount of current is associated with the MSRR Metamaterial structure, which further allows for minimizing the mutual coupling of the antenna array by using the suggested MSRR structure, as shown in Fig.14. The radiation patterns of the suggested antenna array with MSRR Metamaterial structures and without MSRR Metamaterial structures at the operating frequency is illustrated in Fig.15. At the resonance frequency, a small variation in the radiation patterns of antenna arrays can be observed with MSRR Metamaterial structures or without MSRR Metamaterial structures and thereby indicating the suggested MSRR Metamaterial structure to minimize mutual coupling without impacting the properties of radiation. Furthermore, a 1X2 Microstrip patch antenna array

with a 2.4 GHz resonant frequency has been developed and used for the ISM band. Secondly, by employing a modified split ring resonator metamaterial structure as a unit cell, a metamaterial lens is being developed and deployed on the top of the Microstrip patch antenna array. All underlying performance measures are measured without Metamaterial and with Metamaterial during the design optimization process. Polar plots, 3D radiation plots, and S-parameter plots are used to describe the simulation outputs. To increase performance and minimize coupling effects, the metamaterial lens increases, and its antenna gain has increased from 3 to 6.0. At 2.4GHz, a Microstrip Rectangular Patch Antenna, including coaxial feeding, is constructed with the help of FR4 dielectric material with 1.57 mm thickness and with 4.4 dielectric constants. The best possible width, as well as the length of the patch, were found to be 38mm as well as 28mm, respectively. As illustrated in Fig.10, revised metamaterial split ring resonators are positioned 10 mm above a 1 X 2 Microstrip patch antenna array with a spacing of 32 mm between them with 1 mm thickness FR4 dielectric material with 4.4 as the dielectric constant. The MSRR unit cell is made up of two nested rings, and each of these rings consists of two symmetrical splits. The unit cells of MSRR are inserted between the two antennas on the left side with 1 mm spacing between them. Lgnd = 70 mm, L = 28.3 mm, Wgnd = 130 mm, W = 36.5 mm, r1 = 2.5 mm, r2 = 2 mm, d = 31.5 mm, d1 = 0.25 mm, d2 = 0.25 mm, k = 0.08 mm are the best possible antenna array dimensions to obtain maximum isolation and is illustrated in Fig.13. A simulation model in ANSYS HFSS was used to analyze the efficiency of the suggested MSRR loaded antenna array. Fig. 14 illustrates the antenna array return loss with MSRR Metamaterial structures. The antenna array radiation pattern with MSRR Metamaterial structures and the antenna array radiation pattern without MSRR Metamaterial structures. The gain of the suggested antenna array was approximately 6.4 dB, while the gain of a patch array without Metamaterial was 3.7 dB. Compared to a patch array without Metamaterial, the antenna array gain with Metamaterial was nearly doubled. A probe-driven microstrip patch antenna imprinted on an FR4 epoxy substrate with 1.6mm thickness and a dielectric constant of 4.4 is developed in this work via the HFSS tool for wireless applications operating at 2.4GHz. Two hemispherical Teflon lenses with 2.1 as the dielectric constant are inserted just above patches to improve the gain. A mathematical study of spacing between the patches and their placement height is demonstrated. The traditional patch antenna's length, and width, can be estimated. A traditional microstrip patch antenna configuration is imprinted on an FR4 epoxy substrate with 1.6mm thickness and a dielectric constant of 4.4. The dimensions of the patch are 28.3mm x 36.9mm. Coaxial feeding is used to drive the antennas. The spacing between the antennas must be tuned to 62mm to ensure low mutual coupling and optimum gain. Fig.14 shows a 3D representation of the suggested MPA array with the hemispherical lens. Two hemispherical Teflon lenses with 2.1 as the dielectric constant are inserted just above patches to improve the gain. To achieve high gain, the hemispherical lens' height, as well as the radius, must be optimized. The dip is achieved at 2.4GHz and corresponds to the resonant frequency of the traditional patch antenna. At this frequency, the return loss is -19dB and -23.6 dB for the first and second antennae, respectively. The antenna absorbs the maximum input energy whenever the return loss is minimal, i.e., minimum reflection. The gain for MPA, which is simulated via HFSS, is found to be 5.0 dB. This complies with the Microstrip Patch antenna industry benchmark. The initial antenna's resonance frequency is 2.4GHz, and the return loss is -15dB. No resonant frequency modification exists, even though 9dB reduces the return loss. The MPA gain with a hemispherical lens is found to be 11dB. Compared to a traditional patch antenna array, the gain is increased by 7dB. The height at which the hemispherical lens is set is then considered for computational analysis to see how it affects the antenna array's gain. The obtained outcomes are mentioned in the following table. It is seen that whenever the antennas are placed nearer that point, the antenna array gain reduces. This reduction is caused because of the mutual coupling among the array of antennas. Table 1 shows that the gain reduces as the lens position height increases. This is because the lens absorbs fewer electromagnetic waves released by the patches.

4 Conclusion

A simple as well as cost-efficient transmission line phase shifter is presented. A 1 X 2 microstrip patch array antenna operating at 2.6 GHz is built using transmission line feeding. Similarly, an FR4

dielectric substrate with a dielectric constant of 4.4 is employed with a 1.6 mm thickness. By the standard route array antenna, variations in the transmission line feeding approach are measured to produce various phase shift values. Multiple lengths of transmission line feeding are used for the phase shifter. To obtain varied phase shift values, the HFSS simulator tool is employed to develop various sizes of transmission lines. FR4 dielectric substrate with dielectric constant of 4.4 and 1.6 mm thickness is used to create an array of 1 X 2 rectangular microstrip patch antennas operating at a frequency of 2.5 GHz. 36.5 mm, as well as 27.5 mm, are the best possible patch length as well as widths. 193 mm, as well as 73.6 mm, are the length and width of the substrate. We obtained various phase shift values by using a relatively small delay line for the size of the transmission line fed to a 1 X 2 microstrip antenna. Fig. 3 shows how to obtain a $+20^0$-phase shift using a 50.4mm delay line on the right side.
Correspondingly, as illustrated in Fig. 1, a $-+20^0$ phase shift can be obtained by increasing the length of the delay line by 46.4 mm on the left side. The Return loss graph for an antenna array with a $+20^0$ phase shifter design operating at 2.6 GHz is shown in Fig. 2. The red line in Fig. 3 represents a $+20^0$-phase shift value when contrasted to the blue line, which means a standard antenna array. It also shows that the gain for the suggested antenna is roughly 4.8297dB and is depicted in Fig. 4. Return loss graph for an antenna array with a -20^0 phase shifter design operating at 2.6 GHz is shown in Fig. 5. The red line in Fig. 3, represents a -20^0-phase shift value when contrasted to that of the blue line which means a standard antenna array. Fig. 6 shows that the suggested antenna exhibits a gain of approximately 5.0095 dB. In future work, Machine learning and AI-based MPA antenna can be designed to optimize further in terms of mutual coupling effects.

References:

[1] B. Liao and S. C. Chan, "Adaptive beamforming for uniform linear arrays with unknown mutual coupling," *IEEE Antennas and Wireless Propagation Letters*, vol. 11, pp. 464–467, 2012

[2] B. Basu and G. K. Mahanti, "Beam reconfiguration of a linear array of parallel dipole antennas through switching with real excitation voltage distribution," *Annals of Telecommunications*, vol. 67, pp. 285–293, 2012.

[3] M. S. Akyuz, V. B. Erturk, and M. Kalfa, "Closed-form green's function representations for mutual coupling calculations between apertures on a perfect electric conductor circular cylinder covered with dielectric layers," *IEEE Transactions on Antennas and Propagation*, vol. 59, pp. 3094–3098, 2011.

[4] K. Yang, Z. Zhao, Z. Nie, J. Ouyang, and Q. H. Liu, "Synthesis of conformal phased arrays with embedded element pattern decomposition," *IEEE Transactions on Antennas and Propagation*, vol. 59, pp. 2882–2888, 2011.

[5] Al Ka'bi, A.H. The effects of mutual coupling and polarization on the performance of steered-beam adaptive arrays. *J Comput Electron* **20,** 458–466 (2021). https://doi.org/10.1007/s10825-020-01635-x

[6] Al Ka'bi, A.: Performance of adaptive antennas in presence of polarized electromagnetic signals. Telecommun. Radio Eng. **79**(4), 291–304 (2020).

[7] Al Ka'bi, A.H.: Effect of polarization on the performance of adaptive antenna arrays. J. Commun. **15**(9), 661–668 (2020)

[8] Ghaderi, B., Parhizgar, N.: Resource allocation in MIMO systems specific to radio communication. Arch. Electr. Eng. **68**(1), 91–100 (2019).

[9] Jones, J.A., Galvez, J.: The Poincare-Sphere: Approach to Polarization: Formalism and New Labs with Poincare Beams (2018).

[10] Kim Y., Yi D., Yang S., Chae H., Yu J., Myun g N. Beam pattern analysis of antenna array on the complex platform using AEP method based on hybrid UTD-ACGF technique IEEE Trans. Antennas Propag., 65 (3) (2017), pp. 1511-1516

[11] Aziz I, Öjefors E, Dancila D (2021). Connected slots antenna array feeding a high-gain lens for wide-angle beam-steering applications. International Journal of Microwave and Wireless Technologies 1–9. https://doi.org/10.1017/S175907872100012X

[12] A. Artemenko, A. Maltsev, A. Mozharovskiy, A. Sevastyanov, V. Ssorin and R. Maslennikov, "Millimeter-Wave Electronically Steerable Integrated Lens Antennas for

WLAN/WPAN Applications," in IEEE Transactions on Antennas and Propagation, vol. 61, no. 4, pp. 1665-1671, April 2013, DOI: 10.1109/TAP.2012.2232266.

[13] Aziz I, Öjefors E, Dahlbäck R, Rydberg A, Engblom G, and Dancila D (2019) Broadband connected slots phased array feeding a high gain lens antenna at 60 GHz. 2019 49th European Microwave Conference (EuMC). pp. 718–721

[14] K. Xiang and F. Chen, "4 × 4 broadband butler matrix and its application in antenna arrays," in Proceedings of the IEEE International Symposium on Antennas and Propagation and USNC-URSI Radio Science Meeting, pp. 675-676, Atlanta, GA, USA, December 2019.

[15] J. Pang, R. Wu, Y. Wang et al., "A 28-GHz CMOS phased-array transceiver based on LO phase-shifting architecture with gain invariant phase tuning for 5G new radio," IEEE Journal of Solid-State Circuits, vol. 54, no. 5, pp. 1228–1242, 2019.

[16] T. Sowlati, S. Sarkar, B. G. Perumana et al., "A 60-GHz 144- element phased-array transceiver for backhaul application," IEEE Journal of Solid-State Circuits, vol. 53, no. 12, pp. 3640–3659, 2018.

[17] Y. Developpement, "5G's impact on RF front-end module ´ and connectivity for cell phones 2019," 2021, http://www. yole.fr/yole–reports.aspx.